Macromolecules

ARTICLE

pubs.acs.org/Macromolecules

Microstructure and Phase Behavior of POSS/PCL Shape Memory Nanocomposites

Bonifacio Alvarado-Tenorio,[†,‡] Angel Romo-Uribe,[*,‡] and Patrick T. Mather[*,§]

[†]Departamento de Ingeniería Química Metalúrgica, Facultad de Química, Universidad Nacional Autónoma de México, 04510 México D.F., Mexico

[‡]Laboratorio de Nanopolimeros y Coloides, Instituto de Ciencias Fisicas, Universidad Nacional Autónoma de México, Cuernavaca, Mor. 62210, Mexico

[§]Syracuse Biomaterials Institute and Department of Biomedical and Chemical Engineering, Syracuse University, Syracuse, New York 13244, United States

Supporting Information

ABSTRACT: This contribution concerns the microstructure of POSS-based networks previously reported for their shape memory properties [Lee et al. Macromolecules 2008, 41, 4730−4738]. Simultaneous wide-angle and small-angle X-ray scattering (WAXS/SAXS) analysis has revealed highly ordered nanoscale structures in polyhedral silsesquioxane−poly(ε-caprolactone) (POSS-PCL) semicrystalline cross-linked nanocomposites. Architecturally, the oligomers used for network formation resemble a highly asymmetrical triblock copolymer featuring a *single* POSS moiety centered between two PCL chains, yielding two short tethers for a total molecular weight of 2600 g/mol. WAXS patterns of the diol-terminated POSS-PCL sample showed the existence of both crystalline reflections of the PCL orthorhombic phase and crystalline reflections of the POSS rhombohedral phase, indicating microphase separation that allows independent crystallization. Accordingly, two endothermic thermal transitions associated with the melting of each crystal phase were exhibited by the material. Strikingly, SAXS revealed two long period spacings: one associated with the POSS nanobuilding blocks (long period of 66 Å) and the other associated with PCL lamellar nanophase (long period of 151 Å). Surprisingly, end-capping of the PCL alcohol groups with acrylate groups (needed for cross-linking) greatly reduced the crystalline order of POSS nanocages, whereas the orthorhombic phase of PCL remained unchanged. The acrylate groups also produced a significant reduction of melting transition temperature of POSS crystals. Moreover, SAXS showed only one long period (117 Å) associated with PCL crystalline nanostructure. Macromolecular end-linked networks exhibiting shape memory behavior were obtained by photocuring the acrylate-terminated nanocomposites utilizing a tetrathiol cross-linker. Despite the architectural constraints of cross-links, POSS-PCL networks also featured the POSS rhombohedral crystalline phase. However, PCL crystallization was suppressed, resulting in an amorphous PCL phase. DSC analysis of the POSS-PCL networks showed only one endothermic transition. SAXS showed the existence of long-range order in the cross-linked material with the intensity maxima indexed to a cubic lattice with parameter a = 13 nm. That is, a superstructure is present in the cross-linked networks, and the cubic superstructure is attributed to crystalline clusters formed by POSS molecules. To our knowledge, this is the first evidence for such a nanoscale superstructure in a polymer network.

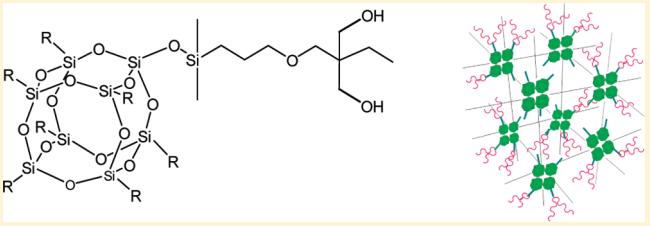

INTRODUCTION

Shape memory polymers (SMPs) are a class of smart materials that respond dynamically to external stimuli like heat,[1−11] electric field,[12−14] magnetic field,[15] infrared radiation,[16−18] and UV radiation.[19,20] Because SMPs can store a temporal shape and return to their original (permanent) shape simply by applying the proper stimulus, these materials have acquired application relevance in a variety of technological fields ranging from medical[2−5,21−25] to aeronautics.[26]

These smart materials have offered technological promise since first reported by the end of the 1970s, where SMPs included cross-linked polyolefins and highly entangled polymers such as polynorbornene (ca. 3×10^6 g/mol).[27] Gradually, the field migrated from the cross-linking of common polymers toward novel compositions and architectures suitable to a wide range of stimuli and even biodegradability. For example, one of us has reported hybrid and biodegradable SMPs from end-linking of low molecular weight (ca. 2000−4000 g/mol) network chains incorporating nanometer size hybrid moieties based on polyhedral oligosilsesquioxanes (POSS).[1−3] Here, POSS is an

Received: March 12, 2011
Revised: May 11, 2011
Published: June 16, 2011

inorganic−organic moiety easily incorporated into polymeric architectures to alter their physical and chemical properties.[28]

Despite extensive study of shape memory phenomena (which is not an intrinsic property of polymers[29−31]) at the macroscopic scale based on thermomechanical cycles,[7−10,32−38] and in consideration of viscoelastic properties, such studies have largely excluded examinations at the micro- and nanoscale, even for crystalline systems. We were motivated to conduct such microstructural studies because an understanding the crystallographic and nanoscale order during the thermomechanical process associated with the shape memory behavior would lead to better control over the mechanisms that rule this behavior. We further suggest that descriptions of shape memory behavior at the microstructural scale is very relevant, especially due to the fact that diverse polymers exhibit this behavior, for instance, cross-linked molecular networks,[1,2,5−7,10,22] block copolymers,[36,37,39] branched polymers,[40] and grafted polymers.[41] Under the appropriate thermomechanical conditions, these polymeric materials will exhibit more or less temporal shape stability—so-called shape "fixing"—and shape recovery to the permanent shape.

Recently, Lee et al.[1] reported on a unique and highly asymmetric system that features a new class of biodegradable hybrid SMP based on polyhedral silsesquioxane (POSS) nanocages, suitable for medical applications. The molecular architecture consisted of a "double network" which features the superposition of a covalent network with a percolative physical network. The covalent network chains featured two polycaprolactone (PCL) chains tethered to a *single* POSS moiety by virtue of its use as a difunctional initiator for PCL ring-opening polymerization. The double networks displayed a shape memory effect up to 42 wt % POSS content, beyond which elastic extensibility was diminished. Wide-angle X-ray scattering demonstrated that the crystallizable moieties, POSS and PCL, gave rise to melting (and crystallization) temperatures suitable for "locking" and activating shape memory behavior. Whereas the coexistence of POSS and PCL crystallites was proven beyond doubt, the micro- and nanoscale ordering was not elucidated, nor was its impact on shape memory behavior investigated.

The characteristics of POSS for the creation of new POSS−polymer systems have been summarized by Wu et al.[42] Those authors described polymeric nanocomposites containing POSS in light of the range of well-defined molecular architectures reported, including (a) amphiphilic POSS telechelics, (b) block copolymers incorporating POSS, and to the less orderly architecture as (c) molecular polymer blends incorporating POSS and (d) POSS-based random copolymers. In the review, the authors summarized the diverse and significant research on POSS-based polymers occurring during the past several years and argued that certain elements of structure−property relationships are prevalent throughout widely varying POSS−polymer systems. In particular, the state of aggregation or crystallization of POSS moieties plays a prominent role in determining such physical properties as viscosity and melt elasticity. Also, connectivity (or not) of POSS to the polymeric host influences microstructure and physical properties in a profound manner.

The crystallographic structure of POSS monomers and polymers has been studied in detail using wide-angle X-ray scattering (WAXS) and transmission electron microscopy (TEM).[43,44] It has been shown that POSS arranges into a rhombohedral (or the equivalent hexagonal) structure and that POSS monomers decorated with alkyl units (or a norbornyl group in place of one alkyl unit) can be treated as spheres packing in the ABCA sequence; i.e., spheres in one layer lie above the interstitial spaces in adjacent layers. The corner units prevent close packing of the spheres, and the nature of the corner units defines the lattice parameters.

Initial studies on POSS-based copolymers were focused on uncrystallizable polymer hosts, and the results showed that at higher concentrations of POSS there was a tendency of pendant POSS moieties to aggregate.[45,46] However, recent studies carried out on POSS−polyethylene copolymers (a crystallizable polymer host) carried out by Coughlin and co-workers[47,48] showed characteristic diffraction reflections demonstrating separate crystallization of POSS and polyethylene (i.e., separate crystal domains). Moreover, on the basis of line broadening measurements, the authors concluded that POSS crystallized as anisotropically shaped crystallites. It is noted that in order to achieve this separate crystallization the molecular weight of the PE-*co*-POSS copolymers ranged from 315 000 to 446 000 g/mol, and POSS concentrations ranged from 19 to 56 wt %. Importantly, Coughlin et al.[48] also reported that the molecular connectivity between POSS and PE provides a source of constraint and frustration for crystallization. Indeed, depending on the recrystallization route followed (cooling from the molten state or solution precipitation), either one species or the other will dominate crystallization. Competitive crystallization within POSS-based copolymers composed of at least one crystallizable species were confirmed for triblock oligomeric copolymers composed of polyethylene (PE), poly(ethylene oxide) (PEO), and polyhedral oligosilsesquioxanes (POSS). Whereas the crystallization of PEO was frustrated due to being attached at both ends to the other two species, the crystallization of PE was either induced or constraint by the crystallization of POSS species. Indeed, POSS crystals actually confine the crystallization of PE, giving rise to once-folded chains, contrary to extended PE chains when the crystallization of PE dominated.[49]

The POSS-PCL system studied here (PCL chains tethered to a *single* POSS moiety) resembles a highly asymmetric block copolymer with crystallizable moieties, resulting in dynamic coupling between crystallization and microphase separation. Such a system offers the possibility to fine-tune the microstructure on the nanometer scale. The present research focused on the investigation at the micro- and nanoscale levels of biodegradable POSS-PCL hybrid nanocomposites exhibiting shape memory behavior, as well as their oligomeric precursors, via simultaneous wide-angle and small-angle X-ray scattering (WAXS/SAXS). The results, correlated with their thermal properties, surprisingly show a highly ordered nanoscale superstructure not only in the precursor but also in the covalently cross-linked networks.

EXPERIMENTAL SECTION

Materials. ε-Caprolactone monomer was vacuum-distilled and stored under nitrogen prior to use. Tin(II) 2-ethylhexanoate catalyst (Aldrich) was also kept under nitrogen. 2-Ethyl-2-[3-[[(heptaisobutyl pentacyclo[9.5.1.1^{50,51}.1^{48,52}.1^{46,53}]octasiloxanyl)oxy]dimethylsilyl]-propoxy]methyl]-1,3-propanediol (or "TMP diolisobutyl-POSS"), hereafter referred to as POSS, was purchased from Hybrid Plastics as a pure (>99%) crystalline solid and used as received. Benzene (anhydrous), triethylamine, acryloyl chloride, 2,2-dimethoxy-2-henylacetophenone, and pentaerythritol tetrakis(3-mercaptopropionate) (hereafter, "tetrathiol") were purchased from Aldrich and used as received. All other solvents were purchased from Fisher Scientific and used without further purification.

Scheme 1. Synthesis Scheme of POSS-Initiated Polycaprolactone Diol[a]

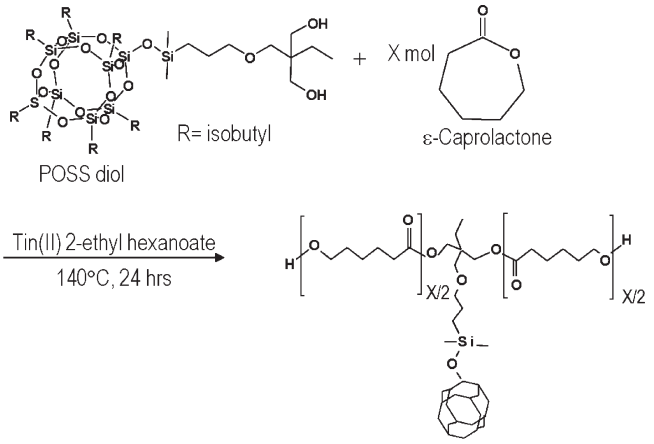

[a] Adapted from ref 1. Note that the POSS cage structure in the macromer is drawn schematically in a simplified form.

Thermal Analysis. Thermal transitions of oligomers and cross-linked networks were characterized by differential scanning calorimetry (DSC) using a Q100 DSC (TA Instruments) instrument. Temperature and heat flow calibrations were carried out using analytical grade indium (T_m = 156.6 °C) and zinc (T_m = 419.5 °C). Samples weighing about 10 mg were loaded into standard aluminum pans. The scans were carried out at 10 °C/min on heating and 5 °C/min on cooling, under a nitrogen atmosphere. Second heating scans are reported after the unknown thermomechanical history of the samples was erased by taking the materials into the molten state. The onset of decomposition temperature, T_{dec}, was determined using a thermogravimetric analyzer Q500 (TA Instruments). Scans were carried out at 10 °C/min under a nitrogen atmosphere.

WAXS/SAXS Analysis. Two-dimensional wide-angle X-ray scattering (WAXS) and small-angle X-ray scattering (SAXS) patterns were obtained using a three-pinhole collimation system, S-Max3000 (Rigaku Inc.) This equipment employs Cu Kα (λ = 1.5405 Å) as the radiation source and was operated at 45 kV and 0.88 mA. WAXS patterns were recorded using a flat-plate camera and Fuji image plates; a sample-to-detector distance of 6 cm was used. The patterns were analyzed using the software POLAR v2.6 (Stonybrook Technology Inc., Stonybrook, NY). SAXS patterns were recorded using an area detector and sample-to-detector distance of 1.1 m. The data were recorded in the range $0.0054 < q < 0.16$ nm^{-1}, where $q = (4\pi/\lambda)\sin\theta$, and 2θ is the scattering angle.

Prior to X-ray analysis, the as-synthesized POSS diols and diacrylate powders were dried at 50 °C for 12 h. The dried powders were then enclosed between Kapton film 50 μm thick. On the other hand, the POSS-PCL networks were first extracted and then dried at 50 °C for 12 h prior to X-ray analysis. Samples were prepared as circular disks of 8.4 mm diameter and 0.3 mm thickness.

RESULTS AND DISCUSSION

The first step toward the POSS-PCL SMP networks was to synthesize POSS-PCL diols. For this, a series of POSS-initiated telechelic diols were synthesized, and the number-average molecular weights, $\overline{M}_n$, ranged from 2600 to 3600 g/mol. The synthesis, microstructure, and thermal properties are reported.

POSS-PCL Diols. The method described by Lee et al.[1] was followed to synthesize POSS-initiated telechelic diols. Purified ε-caprolactone, dried POSS diol, and as-received catalyst tin(II) 2-ethylhexanoate were added to a 100 mL flask under a nitrogen atmosphere, and the mixture was stirred at 140 °C for 24 h. Unreacted material was removed by the following procedure:[1] the resulting telechelic diol liquid was allowed to cool to room temperature, dissolved in tetrahydrofuran (THF), and then precipitated into *n*-hexane, filtered, and dried. The yield for each of these reactions was typically over 90%. The samples are named using the convention P-CL*n*, where *n* indicates the total number-average molecular weight of the diol as prescribed by the feed molar ratio of POSS initiator to ε-caprolactone monomer and measured via ^{1}H NMR using POSS as the internal standard.[1] P-CL*n* diols with number-average molecular weights of 2617, 3246, 3322, and 3592 g/mol were thus synthesized. The synthesis route is depicted in Scheme 1.

The molecular weight and concentration of POSS in the nanocomposites are listed in Table 1. Note that the samples thus synthesized are oligomeric. For instance, the POSS-PCL diol of 3600 g/mol consists of one POSS unit (1052 g/mol) and nine CL repeat units each side, to give a total of 18 CL units (each CL monomer has a molecular weight of 144 g/mol). GPC analysis showed polydispersities of 1.1−1.3, denoting the excellent control in the chemical synthesis. On the other hand, samples with 3246 and 3322 g/mol are effectively identical, as evidenced by their thermal properties shown below, indicating that differences of one CL repeat unit (144 g/mol) are not resolvable. Quantitative ^{1}H NMR data are summarized below.

^{1}H NMR of P-CL2.6 ($CDCl_3$): 0.106 (s, 6H, $-Si-(CH_3)_2$), 0.607 (q, 14H, $-Si-CH_2-CH-$), 0.950 (q, 42H, $-CH-(CH_3)_2$), 1.39 (m, $-CH_2-CH_2-CH_2-$), 1.65 (m, $-CH_2-CH_2-O-$), 1.85 (m, 7H, $-CH-(CH_3)_2$), 2.31 (t, $-OOC-CH_2-CH_2-$), 3.34 (m, $-CCH_2-OOC-$), 3.66 (t, $-CH_2-OH$), 4.06 (t, $-CH_2-CH_2-OOC-$).

Thermal Properties. DSC heating and cooling scans of the POSS-PCL telechelic diols are shown in Figures 1a,b; heating scans corresponding to second heating. The results show that all four POSS-PCL telechelics diols exhibited two well-separated melting (crystallization) transitions. The lower temperature transition is attributed to the PCL tethers ($T_{m,PCL}$), owing to similar melting point reported[22] for PCL oligomers, T_m = 40 °C. On the other hand, the higher temperature transition is attributed to POSS crystalline fraction ($T_{m,POSS}$), given similarity to the neat POSS diol featuring T_m= 130 °C.[2] The presence of both crystalline phases was confirmed by WAXS, as will be discussed in the next section. This existence of two crystalline phases implies PCL-POSS microphase separation, even in oligomeric form.

We observed further that all of the POSS-PCL diols exhibited double or triple lower temperature melting transitions on heating, suggesting a sequence of melting/recrystallizing/melting processes possible in systems associated with significant secondary crystallization.[54,55] Other explanations for multiple melting peaks include the presence of different crystallite sizes of PCL, a crystal-to-crystal transition, or two coexisting crystalline structures.[56] Our experiments are incapable of resolving which of these explanations is the case. The degree of crystallinity associated with the PCL fraction was determined from the corresponding enthalpy of melting, after correcting for the weight fraction of PCL in the diols (known from ^{1}H NMR measurements, Table 1) and taking the heat of fusion of net-PCL to be 126 J/g.[57] In this manner, we found that the degree of crystallinity increased from 34% to 46% as the molecular weight increased.

Thermal analysis also showed that as the molecular weight of the oligomers increased, the melting temperature of the PCL

Table 1. Molecular and Thermal Properties of POSS-PCL Diols

sample	$\overline{M}_n$ (g/mol)	POSS content (mol %/wt %)	$T_{m,PCL}$ (°C) [ΔH_m (J/g)]	$T_{m,POSS}$ (°C) [ΔH_m (J/g)]	$T_{c,PCL}$ (°C) [ΔH_c (J/g)]	$T_{c,POSS}$ (°C) [ΔH_c (J/g)]
P-CL2.6	2600	6.8/40	20 [26]	82 [6.7]	−6 [18]	76 [8]
P-CL3.2	3200	4.9/33	30 [39]	79 [6.4]	2 [38]	69 [7]
P-CL3.3	3300	4.8/32	30 [40]	78 [6.2]	2 [39]	69 [6.7]
P-CL3.6	3600	4.3/29	33 [40]	74 [5.1]	4 [40]	59 [6]

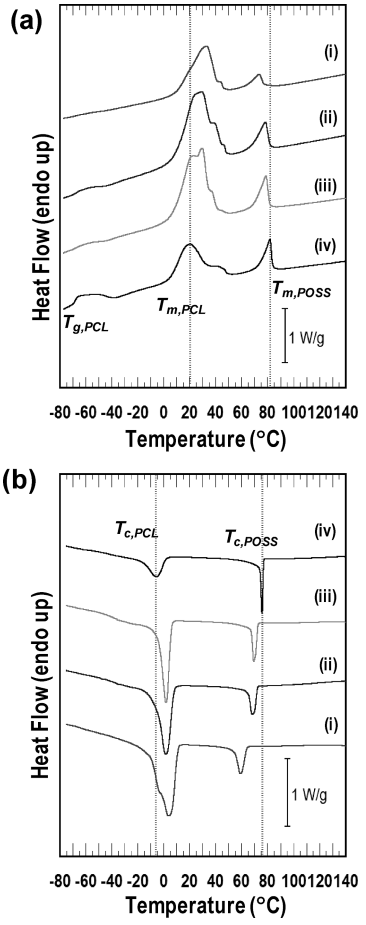

Figure 1. DSC traces of (i) P-CL2.6, (ii) P-CL3.2, (iii) PCL3.3, and (iv) P-CL3.6 diols. (a) Heating (10 °C/min) and (b) cooling (5 °C/min) scans, carried out under a nitrogen atmosphere.

component *increased* (toward the neat PCL melting temperature) whereas the melting temperature of the POSS crystals *decreased*, suggesting competitive crystallization between two phases. The competitive crystallization in copolymers with POSS bonded covalently to crystallizable species has already been reported.[47,49] The thermal analysis results are summarized in Table 1.

WAXS−SAXS Analysis. WAXS diffraction patterns and the corresponding azimuthally averaged intensity traces of (a) neat POSS diol, (b) neat PCL homopolymer (3000 g/mol), and (c) POSS-PCL diol (2600 g/mol) are shown in Figure 2. The WAXS diffraction patterns for all the samples show concentric and sharp reflections with more or less amorphous background consistent with randomly oriented semicrystalline materials. The WAXS pattern of POSS diol (Figure 2a) reveals intense and sharp

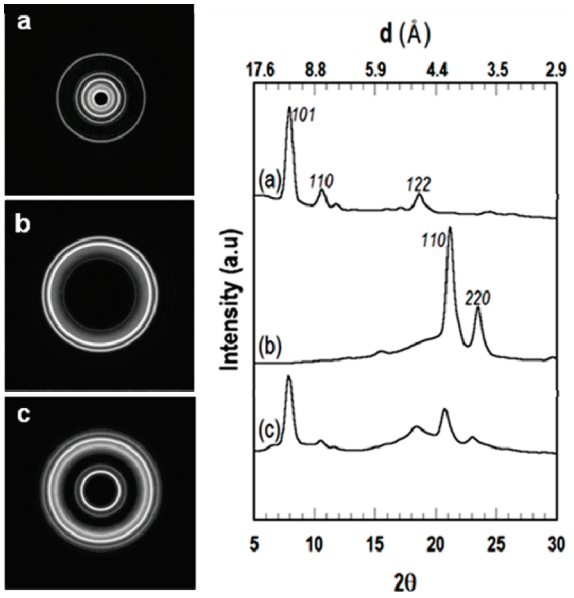

Figure 2. Wide-angle X-ray scattering patterns of (a) neat POSS, (b) neat PCL homopolymer ($\overline{M}_n$ = 3000 g/mol), and (c) P-CL2.6 diol hybrid nanocomposite. The graph on the right shows the corresponding azimuthally averaged intensity traces. Cu Kα radiation.

reflections at $2\theta = 7.9°$ (11.2 Å), 10.6° (8.3 Å), and 18.62° (4.8 Å), which correspond to a rhombohedral[43,44] or equivalently hexagonal crystal unit cell.[43,44] On the other hand, the PCL homopolymer (Figure 2b) shows very sharp crystalline reflections at $2\theta = 21.4°$ (4.15 Å) and 23.6° (3.76 Å), corresponding to (110) and (200) lattice planes of an orthorhombic unit cell.[58−63] Finally, POSS-PCL diol (Figure 2c) showed crystalline reflections for both POSS and PCL; that is, the two crystalline phases coexist in the oligomeric hybrid nanocomposite.

Thus, the WAXS data suggest that there are rhombohedral crystalline entities coexisting with orthorhombic crystals, these crystalline phases being separated spatially and necessarily repeating in space without macroscopic separation prohibited by covalent attachment. Thus, a question arises: does long-range order associated with these crystalline phases exist? As it is known that POSS tends to aggregate, forming crystalline clusters, whereas PCL crystallizes in a chain-folded morphology, it was unclear how such apparently incommensurate arrangements might repeat in the long range.

Small-angle X-ray scattering (SAXS) is an essential tool to reveal realistic microstructural models for nanostructured polymers.[64−66] It is well-known that the contrast mechanism for SAXS is based on the electron density difference between the crystalline and amorphous regions. Commonly, SAXS intensity traces are used to determine the long period or the interlamellar

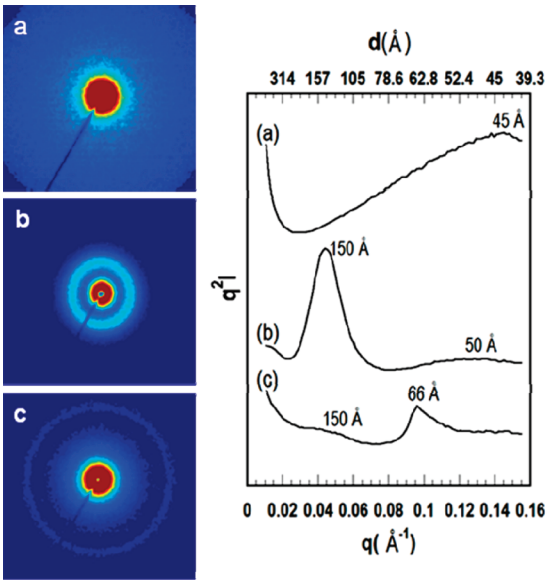

Figure 3. Small-angle X-ray scattering patterns of (a) neat POSS, (b) neat PCL homopolymer ($\overline{M}_n$ = 3000 g/mol), and (c) P-CL2.6 diol hybrid nanocomposite. Lorentz-corrected azimuthally averaged intensity traces. Cu Kα radiation.

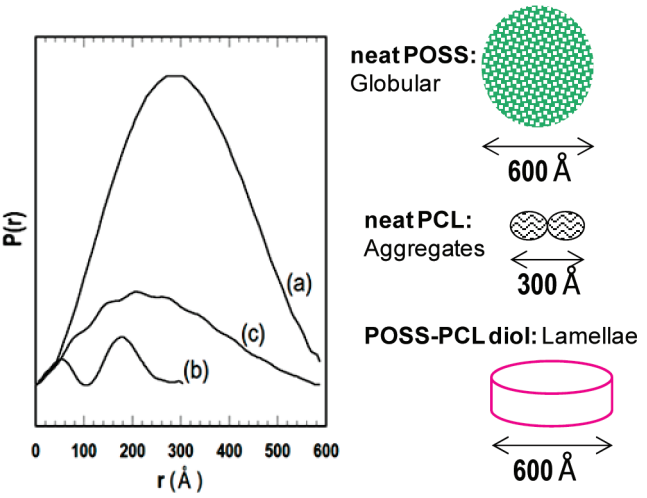

Figure 4. Pair distribution function plots $P(r)$ derived from the SAXS data of (a) neat POSS, (b) neat PCL homopolymer, and (c) P-CL2.6 diol nanocomposite.

spacing directly from the intensity maxima found in the Lorentz corrected plot q^2I vs q.[67−70] Periodic systems should result in individual Gaussian or Lorentzian peaks with the position of a peak maximum indicating the long-range periodicity and the number of peaks indicating the degree of periodicity of the nanostructure.

Figure 3 shows SAXS diffraction patterns and the corresponding Lorentz-corrected plots of (a) neat POSS diol, (b) neat PCL homopolymer (3000 g/mol), and (c) POSS-PCL diol (2600 g/mol). The SAXS trace for neat POSS (Figure 3a) shows an intensity maximum that corresponds to a long period of 45 Å. This long period corresponds well with four interplanar distances d_{hkl} = 11.2 Å (i.e., five rhombohedral unit cells) of the (101) plane, which is observed in its WAXS pattern. According to this result, a rodlike shape, 45 Å in length, is suggested for the neat POSS molecules.

On the other hand, neat PCL homopolymer exhibits two intensity maxima corresponding to long period distances of 151 and 50 Å (Figure 3b). These maxima correspond to first and third orders of reflection for a lamellar morphology.[71−73] It has been shown for SAXS patterns of proteins that a pair of maxima arise from a well-folded structure.[66,74] We suggest, then, that the lamellae in PCL are composed of chains folded only once as the molecular weight of 3000 g/mol has 182 backbone atoms, as determined from alkane structures with similar number of atoms studied by Lord et al.[74] (polyethylene and polycaprolactone both form orthorhombic crystal lattices, and their lattice dimensions are very close, enabling cocrystallization).

Strikingly, the POSS-PCL-2.6 diol showed two SAXS intensity maxima (Figure 3c). First, a weak and broad intensity maximum corresponding to a long period of 151 Å and related to PCL lamellar phase. Then, at higher q value there is a strong intensity maximum corresponding to a long period of 66 Å. It is noted that this long period of 66 Å fits well with six interplanar distances d_{101} = 11.2 Å (i.e., five rhombohedral unit cells) of POSS (101) planes. These results show that in the POSS−PCL hybrid nancomposites two crystalline phases coexist and that two nanostructures representing long-range arrangements of these phases exist, the latter arising from aggregates of POSS and PCL lamellae.

The SAXS data were further analyzed to determine the pair distribution function $P(r)$ (also called the pair-density function).[73,75−77] The $P(r)$ is an autocorrelation function that can be directly calculated through a Fourier transform of the SAXS intensity trace, and the results provide real-space distances associated with electron density distributions in the nanostructured samples. Typically, the $P(r)$ function is calculated by an inverse Fourier transformation to avoid problems due to discrete sampling of the $I(q)$ curve over a finite range.[73] Theoretically, the $P(r)$ function is zero at r = 0 and at $r \geq D_{max}$, where D_{max} corresponds to the maximum linear dimension in the scattering particle. For the processing of real data, the $P(r)$ function is typically constrained in the calculation to be zero at these values; however, this constraint is often not necessary for well-behaved samples and can be an indicator of good quality data. Figure 4 shows the pair distribution functions of (a) neat POSS, (b) neat PCL homopolymer, and (c) the hybrid nanocomposite POSS-PCL diol. The maximum linear dimensions D_{max} and radius of gyration, R_g (where R_g is referring to R_g of the POSS-based repeating superstructure, not individual POSS units), were determined: neat POSS, $D_{max,POSS}$ = 592 Å ($R_{g,POSS}$ = 228 Å); neat PCL, $D_{max,PCL}$ = 305 Å ($R_{g,PCL}$ = 117 Å); and PCL-2.6 diol, $D_{max,P\text{-}CL2.6}$ = 582 Å ($R_{g,P\text{-}CL2.6}$ = 200 Å). All WAXS and SAXS data are summarized in Table 3. We will come back to these dimensions later when a microstructural model is proposed.

POSS-PCL Diacrylate. The POSS-PCL diacrylate (POSS-PCL-DA) sample was synthesized according to the procedure described by Lee et al.[1] For this, the POSS-PCL diol with molecular weight M_n = 2600 g/mol was end-capped with acrylate groups. The yield from the collected POSS-PCL-DA was 90%. The synthesized POSS-PCL-DA was characterized by ^{1}H NMR, as described by Lee et al.,[1] and the average molecular weight was determined to be 2650 g/mol. The weight percent of POSS present in the as-synthesized POSS-PCL-DA was 39 wt %. Scheme 2 shows the synthesis procedure for POSS-PCL-DA.

dx.doi.org/10.1021/ma2005662 |*Macromolecules* 2011, 44, 5682–5692

Scheme 2. Synthesis Scheme of the POSS–Polycaprolactone Diacrylate Macromer (Adapted from Ref 1)

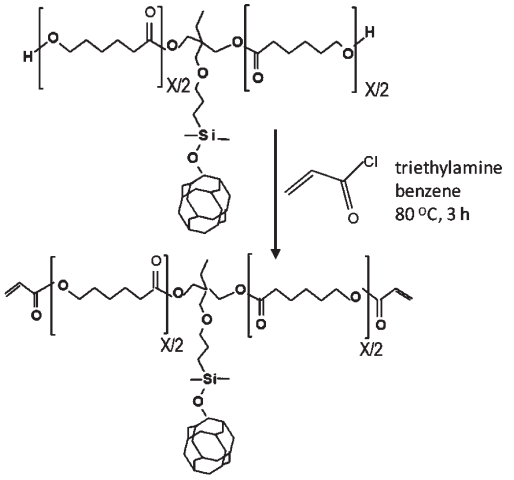

Thermal Properties. The melting and crystallization temperature of the POSS-PCL-DA hybrid nanocomposite determined by DSC, and compared with its precursor POSS–PCL diol, is shown in Figure 5. The second heating scan (Figure 5a, trace ii) showed a very strong sharp endotherm that corresponds to PCL crystalline fraction, with $T_{m,PCL}$ = 45 °C (ΔH_m = 62 J/g). There was also a very small endotherm appearing on the high temperature shoulder of this strong endotherm. The small endotherm features a temperature of $T_{m,POSS}$ = 54 °C, and despite its low temperature, we relate this to the melting of a POSS crystalline fraction. This assumption is supported by the results from the cooling scan (Figure 5b, trace ii) where there can be seen two exotherms of crystallization clearly defined. Further support from WAXS will be shown below. The relative crystallinity (a fraction of the total degree of crystallinity attributed just to PCL), χ, of PCL end-capped with acrylate groups increased significantly when compared to the crystallinity in the POSS-PCL diol (PCL-2.6). The crystallinity, as determined using the enthalpy of crystallization value, resulted in χ_{PCL} = 82%, which is more than double that of the diol (χ_{PCL} = 34%).

Our DSC results also showed that both crystalline phases displayed supercooling, with the recrystallization of POSS occurring at $T_{c,POSS}$ = 40 °C ($\Delta H_{c,POSS}$ = 3.2 J/g), while PCL exhibited a temperature of crystallization of $T_{c,PCL}$ = 27 °C ($\Delta H_{c,PCL}$ = 55 J/g). By comparing the DSC thermograms from POSS-PCL diol (trace i) to that of POSS-PCL diacrylate (trace ii), it is clear that the substitution of diol groups (−OH) with acrylate groups (−O−CO−CH=CH_2) strongly compromised the crystallization of POSS.

The observed difference in crystallinity in the diols and acrylate oligomers can be explained by inter- and intramolecular interactions produced in each of these nanohybrid oligomers, as evidenced by the FTIR spectra, specifically by the formation of hydrogen bonding (Figure S3, Supporting Information). It was observed, in the range 3000−4000 cm^{-1}, a hydroxyl band at 3530 cm^{-1}, which corresponds to *intramolecular* hydrogen bonding, and a second hydroxyl band at 3438 cm^{-1}, which is associated with *intermolecular* hydrogen bonding.[78] Each of these hydrogen bonds may favor the crystallization of either POSS or PCL in each oligomer. We suggest that the intermolecular hydrogen bond in the nanohybrid diol is the dominant

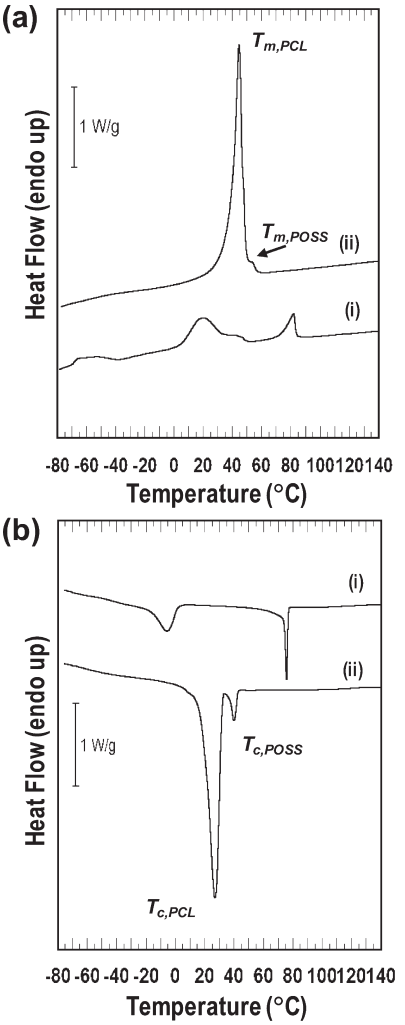

Figure 5. DSC thermograms of (i) P-CL2.6 diol and (ii) P-CL2.6 acrylate hybrid macromers. (a) Heating (10 °C/min) and (b) cooling (5 °C/min) scans, carried out under a nitrogen atmosphere.

interaction, and it arises from the interaction of the PCL hydroxyl end groups (hydrogen bond donors) and the oxygen acceptors in POSS cage structure. This interaction would restrict the ordering of the PCL chains compromising the crystallization, as evidenced by calorimetry and X-ray scattering results.

On the other hand, the diacrylate oligomer methylene has π-bonds that can interact with an adjacent carbonyl group, yielding an intramolecular hydrogen bond producing a ring structure of four atoms. This intramolecular arrangement would not interefere with the ordering of PCL chains to form crystals as well as long-range structures (lamellae), as shown by the calorimetry and X-ray scattering results.

WAXS–SAXS Analysis. WAXS and SAXS measurements were carried out on the hybrid diacrylate oligomer (Figures 6 and 7, respectively) to investigate the effect of the acrylate substitution on the crystal and nanostructure order. Figure 6 shows the WAXS pattern and the azimuthally averaged intensity trace. The results still show the crystalline reflections associated with POSS; however, these reflections have weakened and broadened significantly. For instance, the full width at half-maximum (fwhm) of the 101 (7.9° 2θ) reflection of POSS has increased from 0.30° in the diol to 0.66° in the diacrylate. Using the Scherrer equation, this

dx.doi.org/10.1021/ma2005662 |*Macromolecules* 2011, 44, 5682–5692

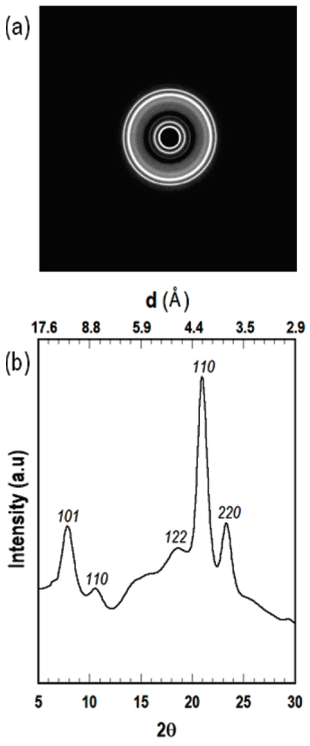

Figure 6. (a) Wide-angle X-ray scattering pattern and (b) azimuthally averaged wide-angle X-ray scattering trace of P-CL2.6 diacrylate hybrid macromer. Cu Kα radiation.

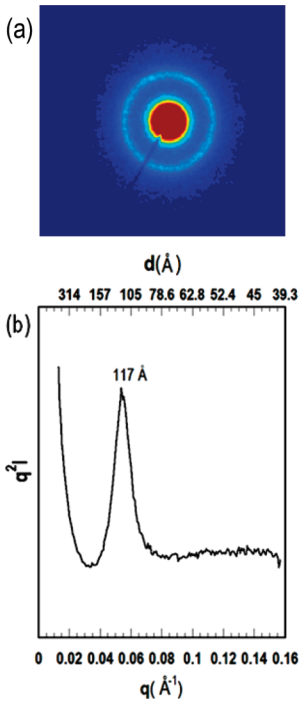

Figure 7. (a) Small-angle X-ray scattering pattern and (b) Lorentz-corrected azimuthally averaged intensity trace of P-CL2.6 acrylate hybrid macromer. Cu Kα radiation.

fwhm values translate to average crystal thicknesses of 258 and 142 Å, respectively, indicating nearly 50% reduction in crystal size (fwhm and crystal thickness are reciprocal). The weakened crystalline reflections of POSS are consistent with the very weak melting observed by DSC discussed above in reference to Figure 5a, trace ii.

The WAXS results also show that the crystallization of PCL dominates the microstructure of the acrylate-capped hybrid oligomers, the 110 PCL interchain reflection being about 3 times as intense as the 101 POSS reflection. This is quite different from the diols case where POSS' 101 reflection was about twice the intensity of PCL's 110 reflection (Figure 2c). These results again are consistent with the very strong endothermic peak of PCL observed by DSC (Figure 5a, trace ii). Looking closely at the fwhm values for the 110 reflection, it was determined that the average thickness of PCL crystals was slightly reduced, from 218 Å (diol) to 172 Å in the diacrylate-capped hybrid oligomers.

Insight into the nanostructure of the diacrylate-capped hybrid oligomers was obtained using small-angle X-ray scattering. The SAXS pattern and azimuthally averaged Lorentz-corrected intensity trace are shown in Figure 7 a,b. The results show a surprisingly distinct long-range halo, the intensity maximum giving a long period of 117 Å. Whereas in the case of the diol nanocomposite there were two nanostructures coexisting (PCL lamellar and POSS aggregates), in the case of the diacrylate there is only one nanoscale superstructure apparent. From the lamellar structure of PCL it is possible to work out the nanostructure that gives rise to this long periodicity. It was established earlier that PCL with molecular weight 2650 g/mol is folded only once per chain. On the other hand, Lord et al.[74] have reported that the alkanes crystallize in lamellae with a tilting angle of 35°

Scheme 3. Proposed Long-Range Order of P-CL2.6 Acrylate Hybrid Nanocomposites According to WAXS and SAXS Results

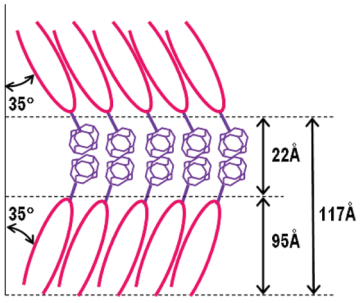

between the chain backbone and the lamellae normal. Thus, the lamellae thickness is obtained from the product (cos 35° × 117 Å) = 95 Å. There is, therefore, a difference of 22 Å, which is assumed to be composed of two 101 plane distances of POSS molecules; a sketch of this proposed repeating structure is shown in Scheme 3. The fact that both POSS and PCL compose the same nanostructure means that both crystalline species must melt at nearly the same temperature, as observed by DSC (Figure 5, trace ii).

To analyze the nanostructure of POSS−PCL diacrylate in more detail, the pair distribution function, $P(r)$, was determined from the SAXS data. It was found that the $P(r)$ of POSS−PCL dicrylate indeed intercepted the y-axis at the origin, which indicated good resolution of the SAXS scattering trace. From the $P(r)$ profile (results available in Supporting Information), the maximum linear dimension D_{max} and radius of gyration R_g of the particles were calculated resulting in $D_{max,P\text{-}CL\text{-}A}$ = 592 Å and

dx.doi.org/10.1021/ma2005662 |*Macromolecules* 2011, 44, 5682–5692

$R_{g,P\text{-}CL\text{-}A}$ = 228 Å. We note the absence of any significant reduction in D_{max} and R_g relative to the POSS−PCL diol.

POSS-PCL Cross-Linked Networks. In order to obtain photocured POSS−PCL networks, a tetrathiol cross-linker pentaerythritol tetrakis(3-mercaptopropionate) (hereafter, "tetrathiol") was used to end-link POSS-PCL diacrylate oligomers under photoinitiated thiol−acrylate addition and minor free radical polymerization.[79] The influence of the degree of cross-linking was investigated, as the diacrylate:tetrathiol molar ratio was varied to include 2:1 (stoichiometric), 2:1.5, and 2:2. After photocuring, the resulting covalent networks were optically transparent and soft at room temperature. Figure 8 shows pictures of the as-cured samples, and their properties are summarized in Table 2. The increase of tetrathiol cross-linker molar ratio affected significantly the gel fraction of the POSS-polycaprolactone network photocured. According to the diacrylate:tetrathiol molar ratio used (2:1, 2:1.5, and 2:2), the synthesized networks exhibited 87%, 75%, and 67% gel fraction after they were extracted, respectively.

Thermal Properties. Figure 9 shows the (a) heating and (b) cooling scans of the POSS-PCL networks. Surprisingly, the cross-linked networks exhibited a well-defined melting transition despite the architectural constraints of cross-links. The corresponding melting temperatures (and enthalpies) of the networks were (i) $T_{m,2:1}$ = 30 °C ($\Delta H_{m,2:1}$ = 3.3 J/g), (ii) $T_{m,\ 2:1.5}$ = 32 °C ($\Delta H_{m,\ 2:1.5}$ = 3.0 J/g), and (iii) $T_{m,2:2}$ = 36 °C ($\Delta H_{m,2:2}$ = 2.5 J/g). The highest molar concentration of the tetrathiol cross-linker yielded the highest melting temperature of the network. Note that the network prepared with the highest molar concentration of tetrathiol, PCL-net-2:2 (trace iii), melts at a temperature very close to the human body temperature (37 °C), a result of potential importance in for biomedical applications. Figure 9b shows the cooling DSC scans for the networks. The corresponding crystallization temperatures (and enthalpies) were found to be (i) $T_{c,2:1}$ = 16 °C ($\Delta H_{c,2:1}$ = 2.2 J/g), (ii) $T_{c,2:1.5}$ = 18 °C ($\Delta H_{c,2:1.5}$ = 2.2 J/g), and (iii) $T_{c,2:2}$ = 21 °C ($\Delta H_{c,2:2}$ = 2.2 J/g). In summary, it is important to note that the melting temperature of the networks ranged from 30 to 36 °C just by increasing the concentration (molar ratio) of the tetrathiol cross-linker. The thermal analysis results raised the question as what is the microstructure melting in the cross-linked networks. We address it by carrying out X-ray scattering experiments.

WAXS−SAXS Analysis. WAXS patterns were obtained for each photocured covalent network, and a typical pattern and the azimuthally averaged intensity traces for the three networks are shown in Figure 10a,b. The pattern, obtained from the P-CL2.6-net-2:1 network, shows sharp inner crystalline reflections and an outer rather broad amorphous halo. These features are shown more clearly in the radial intensity traces shown in Figure 10b. The intensity traces correspond to (i) P-CL2.6-net-2:1, (ii) P-CL2.6-net-2:1.5, and (iii) P-CL2.6-net-2:2. The more intense crystalline reflection corresponds to the (101) reflection (indexed for a rhombohedral crystal lattice) of POSS nanobuilding blocks. On the other hand, the broad amorphous halo centered around 2θ = 19° corresponds to PCL amorphous phase. Thus, these WAXS results indicate that there are POSS crystals embedded within an amorphous PCL phase and that the endothermic (exothermic) peak observed by DSC (Figure 9a,b) corresponds to the melting (recrystallization) of these POSS crystals. This melting point for a POSS crystal is the lowest ever reported, to our knowledge, and reflects the particular arrangement within amorphous PCL.

In order to inspect the long-range, nanoscale order of the POSS-PCL networks, SAXS patterns were also collected. The

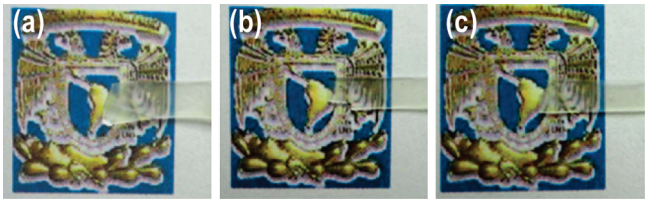

Figure 8. Photographs of photocured POSS-PCL networks with molar ratios (a) 2:1, (b) 2:1.5, and (c) 2:2. The sample dimensions are (a) 3.2 mm × 0.3 mm × 9.1 mm; (b) 2.6 mm × 0.3 mm × 9 mm; and (c) 2.8 mm × 0.3 mm × 9 mm.

Table 3. Crystalline and Nanostructure Characteristics of Neat POSS, Neat PCL Homopolymer, and Their Corresponding POSS-PCL Hybrid Nanocomposites Obtained from Wide- and Small-Angle X-ray Scattering

	WAXS		SAXS			
sample	L_{PCL}[a] (Å)	L_{POSS}[a] (Å)	d_{PCL}[b] (Å)	d_{POSS}[b] (Å)	D_{max}[c] (Å)	R_g[c] (Å)
POSS		286		45	592	228
PCL3k	261		151		305	117
P-CL2.6	218	258	150	66	582	200
P-CL2.6-DA	172	142	117		592	228
P-CL2.6-net-2:1		131		75, 45	586	213
P-CL2.6-net-2:1.5		127		46	589	216
P-CL2.6-net-2:2		127		46	586	215

[a] Average crystal thickness calculated using the Scherrer equation. [b] Long period or interlamellar distance from the principal peak of the Lorentz-corrected plot $q^2I(q)$ vs q. [c] Parameters obtained from the pair distribution function plot $P(r)$ vs r of the SAXS profile.

Table 2. Molecular Characteristics and DSC Results of POSS-PCL Acrylate (P-CL-A) and POSS-PCL Networks Synthesized from POSS-PCL Diol Having an Average Molecular Weight of 2600 g/mol and POSS Content 40 wt %

sample	P-CL-A:cross-linker ratio	gel fraction (%)	$T_{m,PCL}$ (°C) [ΔH_m (J/g)]	$T_{m,POSS}$ (°C) [ΔH_m (J/g)]	$T_{c,PCL}$ (°C) [ΔH_c (J/g)]	$T_{c,POSS}$ (°C) [ΔH_c (J/g)]
P-CL2.6			20 [26]	82 [6.7]	−6 [18]	76 [8.0]
P-CL2.6-A			45 [62]	54	27 [55]	40 [3.2]
P-CL2.6-net-2:1	2:1.0	87		30 [3.3]		16 [2.2]
P-CL2.6-net-2:1.5	2:1.5	75		32 [3.0]		18 [2.2]
P-CL2.6-net-2:2	2:2.0	66		36 [2.5]		21 [2.2]

dx.doi.org/10.1021/ma2005662 |*Macromolecules* 2011, 44, 5682–5692

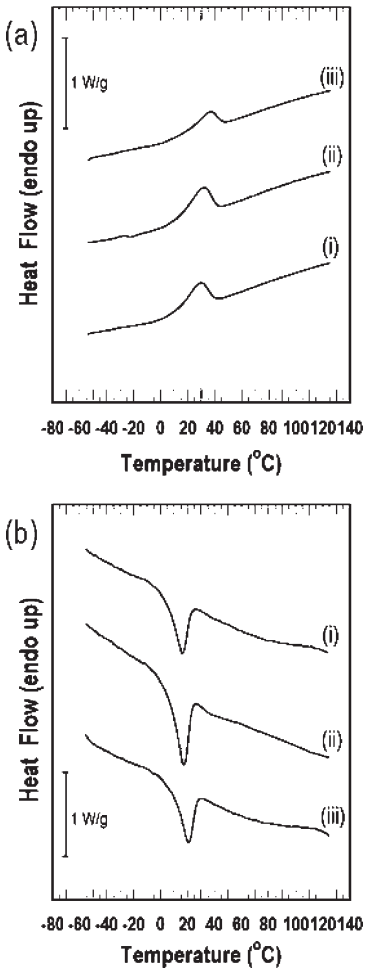

Figure 9. DSC thermograms of POSS-PCL networks: (i) P-CL2.6-net-2:1, (ii) P-CL2.6-net-2:1.5, (iii) P-CL2.6-net-2:2. (a) Heating scans and (b) cooling scans, under a nitrogen atmosphere.

Lorentz-corrected SAXS intensity traces are shown in Figure 11. The inset shows a SAXS pattern of the P-CL2.6-net-2:1 network, clearly revealing well-defined, long-range structure. The sample P-CL2.6-net-2:1 (trace (iii) exhibits two intensity maxima positioned at q_{max} = 0.0839 and 0.138 37 Å^{-1}, which correspond to the long-range distances d = 75 Å and d = 46 Å, as obtained from $q_{max} = 2\pi/d$. On the other hand, the other two networks showed only the intensity maximum at 0.138 37 Å^{-1}. The nanostructure giving rise to these SAXS patterns was worked out by assuming a simple cubic unit cell, where the interplanar distances are given by $d_{111} = a/\sqrt{3}$, $d_{200} = a/2$, and $d_{220} = a/(2\sqrt{2})$. The parameter a would be 130 Å, and considering the interplanar distances ratio $1:\sqrt{3}/2:(3/2)^{1/2}/2$, we can see that the interplanar distances d = 75 Å and d = 46 Å fit well to a cubic structure. The interplanar distances ratio results in 75 Å:65 Å:46 Å, where d_{200}= 65 Å is probably overlapping in the SAXS trace.

In the forgoing, our SAXS results suggest that POSS crystals are arranged into a cubic superstructure and surrounded by an amorphous PCL phase; this assumption is supported from the POSS crystalline reflections from WAXS. A sketch of the suggested nanostructure is shown in Scheme 4. The pair distribution functions were also determined from the SAXS data (Figure S3, Supporting Information), and the maximum linear dimension D_{max} and radius of gyration R_g were calculated for each sample: $D_{max,PCL2.6\text{-}net\text{-}2:1}$ = 586 Å ($R_{g,PCL2.6\text{-}net\text{-}2:1}$ = 213 Å), $D_{max,PCL2.6\text{-}net\text{-}2:1.5}$ = 589 Å ($R_{g,PCL2.6\text{-}net\text{-}2:1.5}$ = 216 Å, and $D_{max,PCL2.6\text{-}net\text{-}2:2}$ = 586 Å ($R_{g,PCL2.6\text{-}net\text{-}2:2}$ = 215 Å).

The generalized indirect Fourier transformation results in the pair distribution functions, $P(r)$ (Figure S3, Supporting

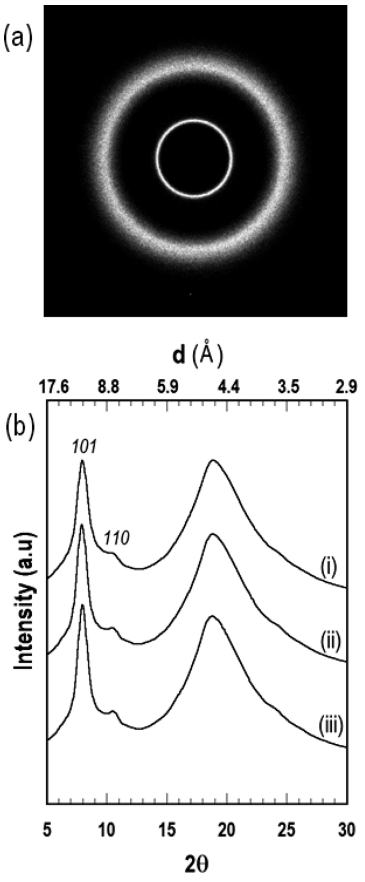

Figure 10. Azimuthally averaged wide-angle X-ray scattering patterns for (i) P-CL2.6-net-2:1, (ii) P-CL2.6-net-2:1.5, and (iii) P-CL2.6-net-2:2.

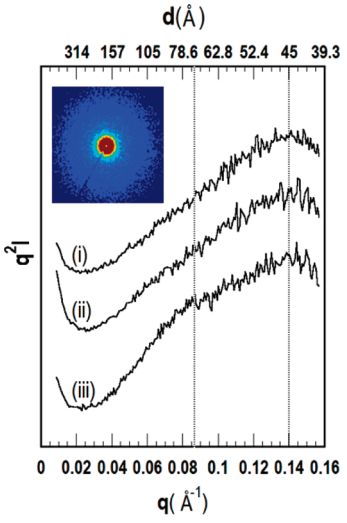

Figure 11. Azimuthally averaged small-angle X-ray scattering traces for (i) P-CL2.6-net-2:2, (ii) P-CL2.6-net-2:1.5, and (iii) P-CL2.6-net-2:1.

dx.doi.org/10.1021/ma2005662 |*Macromolecules* 2011, 44, 5682–5692

Scheme 4. Proposed Cubic Superstructure for the Network P-CL2.6-net-2:1 Derived from SAXS Data

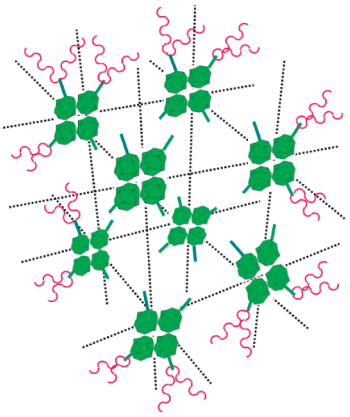

Information), are typical of globular objects with liquidlike packing.[80] Neither curve is completely symmetrical, which can be explained by either a size distribution function or a deviation from a perfect spherical shape. It is noted that the globular morphology is present since the POSS monomer (Figure 4, trace a) and preserved for the diols, diacrylates (Figure S2), and networks, with no change in the maximum linear dimension. Thus, it appears that POSS drives the nanostructure in the hybrid nanocomposites and molecular networks.

CONCLUSIONS

In this research, we have elucidated the ordered spatial arrangement at the micro and nanoscale in the shape memory PCL-POSS cross-linked networks and in their synthesis precursors (POSS-PCL diol and diacrylate hybrid oligomers). It was observed that for POSS-PCL diols there is coordination (via hydrogen bonding) between the inert corner groups of POSS and the PCL end groups, thus compromising PCL crystallization. Thus, the nanostructure was dominated by POSS crystallization. Strikingly, end-capping had a significant impact on POSS crystallization. End-capping prevented the coordination between the corner groups of POSS and the PCL end groups thus freeing PCL chains for fold crystallization. Therefore, PCL dominated the crystallization and nanostructure, as evidenced by calorimetry and X-ray scattering. On the other hand, network formation gave rise to POSS crystals embedded in an amorphous PCL phase. Moreover, POSS was segregated to form crystalline clusters that organized into a surprisingly highly ordered (cubic) superstructure. The findings of this research offer the possibility to fine-tune well-ordered nanostructures from highly asymmetric POSS-based macromers, where there is control over the structure and advantage is taken of end group reactivity to form networks.

ASSOCIATED CONTENT

Supporting Information. Pair distribution function plot $P(r)$ derived from the SAXS data of P-CL2.6-DA nanocomposite; pair distribution function plots $P(r)$ derived from the SAXS data of cross-linked networks: (a) P-CL2.6-net-2:1, (b) P-CL2.6-net-2:1.5, (c) P-CL2.6-net-2:2; FTIR spectra in the 4000−3000 cm^{-1} wavenumber region of (a) P-CL2.6 diol and (b) P-CL2.6-DA diacrylate hybrid nanocomposites. This material is available free of charge via the Internet at http://pubs.acs.org.

AUTHOR INFORMATION

Corresponding Author

*E-mail: aromo-uribe@fis.unam.mx (A.R.-U.), ptmather@syr.edu (P.T.M.).

ACKNOWLEDGMENT

The authors are thankful to Prof. Simon Hanna (University of Bristol, UK) for enlightening discussions pertaining to the crystallization of POSS and PCL. B. Alvarado-Tenorio was supported by a graduate scholarship from the Mexican Council for Science and Technology (CONACyT). This research was partially supported by CONACyT (CIAM2006, grant 58646) and the NSF under the Colaboracion Interamericana de Materiales and the Materials World Network (DMR-0758631) programs.

REFERENCES

(1) Lee, K. M.; Knight, P. T.; Chung, T.; Mather, P. T. *Macromolecules* **2008**, *41*, 4730–4738.
(2) Knight, P. T.; Lee, K. M.; Chung, T.; Mather, P. T. *Macromolecules* **2009**, *42*, 6596–6605.
(3) Knight, P. T.; Lee, K. M.; Qin, H.; Mather, P. T. *Macromolecules* **2008**, *9*, 2458–2467.
(4) Alteheld, A.; Feng, Y.; Kelch, S.; Lendlein, A. *Angew. Chem., Int. Ed.* **2005**, *44*, 1188–1192.
(5) Choi, N.-Y.; Kelch, S.; Lendlein, A. *Adv. Eng. Mater.* **2006**, *8*, 439–445.
(6) Bellin, I.; Kelch, S.; Robert, L.; Lendlein, A. *Proc. Natl. Acad. Sci. U.S.A.* **2006**, *103*, 18043–18047.
(7) Chung, T.; Romo-Uribe, A.; Mather, P. T. *Macromolecules* **2008**, *41*, 184–192.
(8) Xie, T.; Rousseau, I. A. *Polymer* **2009**, *50*, 1852–1856.
(9) Jeon, H. G.; Mather, P. T.; Haddad, T. S. *Polym. Int.* **2000**, *49*, 453–457.
(10) Liu, C.; Chun, S. B.; Mather, P. T.; Zheng, L.; Haley, E. H.; Coughlin, E. B. *Macromolecules* **2002**, *35*, 9868–9874.
(11) Neffe, A. T.; Hanh, B. D.; Steuer, S.; Lendlein, A. *Adv. Mater.* **2009**, *21*, 3394–3398.
(12) Paik, I. H.; Goo, N. S.; Jung, Y. C.; Cho, J. W. *Smart Mater. Struct.* **2006**, *15*, 1476–82.
(13) Koerner, H.; Price, G.; Pearce, N.; Alexander, M.; Vaia, R. A. *Nature Mater.* **2004**, *3*, 115–120.
(14) Leng, J. S.; Huang, W. M.; Lan, X.; Liu, Y. J.; Du, S. Y. *Appl. Phys. Lett.* **2008**, *92*, 204101.
(15) Buckley, P. R.; McKinley, G. H.; Wilson, T. S.; Small, W.; Benett, W. J.; Bearinger, J. P.; McElfresh, M. W.; Maitland, D. J. *IEEE Trans. Biomed. Eng.* **2006**, *53*, 2075–2083.
(16) Mohr, R.; Kratz, K.; Weigel, T.; Lucka-Gabor, M.; Moneke, M.; Lendlein, A. *Proc. Natl. Acad. Sci. U.S.A.* **2006**, *103*, 3540–3545.
(17) Ahir, S. V.; Terentjev, E. M. *Nature Mater.* **2005**, *4*, 491–495.
(18) Vaia, R. *Nature Mater.* **2005**, 429–430.
(19) Lendlein, A.; Jiang, H. Y.; Junger, O.; Langer, R. *Nature* **2005**, *434*, 879–882.
(20) Jiang, H. Y.; Kelch, S.; Lendlein, A. *Adv. Mater.* **2006**, *18*, 1471–1475.
(21) Small, W., IV; Wilson, T.; Benett, W. J.; Loge, J. M.; Maitland, D. J. *Opt. Express* **2005**, *13*, 8204–8213.
(22) Lendlein, A.; Langer, R. *Science* **2002**, *296*, 1673–1676.
(23) Metcalfe, A.; Desfaits, A.-C.; Salazkin, I.; Yahia, L.; Sokolowskic, W. M.; Raymond, J. *Biomaterials* **2003**, *24*, 491–497.
(24) Wache, H. M.; Tartakowska, D. J.; Hentrich, A.; Wagner, M. H. *J. Mater. Sci.: Mater. Med.* **2004**, *14*, 109–112.
(25) Baer, G. M.; Small, W., IV; Wilson, T. S.; Benett, W. J.; Matthews, D. L.; Hartman, J.; Maitland, D. J. *Biomed. Eng. Online* **2007**, *6*, 43–47.

(26) Lan, X.; Liu, Y.; Lv, H.; Wang, X.; Leng, J.; Du, S. *Smart. Mater. Struct.* **2009**, *18*, 024002.
(27) Sakurai, K.; Takahashi, T. *J. Appl. Polym. Sci.* **1989**, *38*, 1191–1194.
(28) Li, G.; Wang, L.; Ni, H.; Pittman, C. U., Jr. *J. Organomet. Polym.* **2001**, *11*, 123–154.
(29) Lendlein, A.; Kelch, S. *Angew. Chem., Int. Ed.* **2002**, *41*, 2034–2057.
(30) Liu, C.; Qin, H.; Mather, P. T. *J. Mater. Chem.* **2007**, *17*, 1543–1558.
(31) Gunes, I. S.; Jana, S. C. *J. Nanosc. Nanotechnol.* **2008**, *8*, 1616–1637.
(32) Qin, H.; Mather, P. T. *Macromolecules* **2009**, *42*, 273–280.
(33) Rousseau, I. A.; Mather, P. T. *J. Am. Chem. Soc.* **2003**, *125*, 15300–15301.
(34) Xu, J. W.; Shi, W. F.; Pang, W. M. *Polymer* **2006**, *47*, 457–465.
(35) Cho, T. K.; Chong, M. H.; Chun, B. C.; Kim, H. R.; Chung, Y.-C. *Fiber Polym.* **2007**, *8*, 7–12.
(36) Lee, B. S.; Chun, B. C.; Chung, Y. C.; Sul, K. I.; Cho, J. W. *Macromolecules* **2001**, *34*, 6431–6437.
(37) Kim, B. K.; Shin, Y. J.; Cho, S. M.; Jeong, H. M. *J. Polym. Sci., Part B: Polym. Phys.* **2000**, *38*, 2652–2657.
(38) Jeong, H. M.; Ahn, B. K.; Kim, B. K. *Eur. Polym. J.* **2001**, *37*, 2245–2252.
(39) Lee, H. Y.; Jeong, H. M.; Lee, J. S.; Kim, B. K. *Polym. J.* **2000**, *32*, 23–28.
(40) Takahashi, T.; Hayashi, N.; Hayashi, S. *J. Appl. Polym. Sci.* **1996**, *60*, 1061–1069.
(41) Li, F.; Chen, Y.; Zhu, W.; Zhang, X.; Xu, M. *Polymer* **1998**, *39*, 6929–6934.
(42) Wu, J.; Mather, P. T. *J. Macromol. Sci., Polym. Rev.* **2009**, *49*, 25–63.
(43) Fu, B. X.; Hsiao, B. S.; White, H.; Rafailovich, M.; Mather, P. T.; Jeon, H. G.; Phillips, S.; Lichtenhan, J. D.; Schwab, J. *Polym. Int.* **2000**, *49*, 437–440.
(44) Waddon, A. J.; Coughlin, E. B. *Chem. Mater.* **2003**, *15*, 4555–4561.
(45) Romo-Uribe, A.; Mather, P. T.; Haddad, T. S.; Lichtenhan, J. D. *J. Polym. Sci., Polym. Phys.* **1998**, *36*, 1857–1872.
(46) Mather, P. T.; Jeon, H. G.; Romo-Uribe, A.; Haddad, T. S.; Lichtenhan, J. D. *Macromolecules* **1999**, *32*, 1194–1203.
(47) Zheng, L.; Waddon, A. J.; Farris, R. J.; Coughlin, E. B. *Macromolecules* **2002**, *35*, 2375–2379.
(48) Waddon, A. J.; Zheng, L.; Farris, R. J.; Coughlin, E. B. *Nano Lett.* **2002**, *2*, 1149–1155.
(49) Miao, J.; Cui, L.; Lau, H. P.; Mather, P. T.; Zhu, L. *Macromolecules* **2007**, *40*, 5460–5470.
(50) Maiti, P.; Batt, C. A.; Giannelis, E. P. *Biomacromolecules* **2007**, *8*, 3393–3400.
(51) Lichtenhan, J. D.; Otonari, Y. A.; Carr, M. J. *Macromolecules* **1995**, *28*, 8435–8437.
(52) Liu, L.; Qi, Z.; Zhu, X. *J. Appl. Polym. Sci.* **1999**, *71*, 1133–1138.
(53) Hong, B.; Thoms, T. P. S.; Murfee, H. J.; Lebrun, M. J. *Inorg. Chem.* **1997**, *36*, 6146–6147.
(54) Wunderlich, B. In *Macromolecular Physics, Crystal Nucleation, Growth, Annealing*; Academic Press: New York, 1976; Vol. 2, p 168.
(55) An, J. H.; Kim, H. S.; Chung, D. J.; Lee, D. S.; Kim, S. *J. Mater. Sci.* **2001**, *36*, 715–722.
(56) Takizawa, K.; Tang, C.; Hawker, C. J. *J. Am. Chem. Soc.* **2008**, *130*, 1718–1726.
(57) *Polymer Data Handbook*; Oxford University Press, Inc.: Oxford, UK, 1999.
(58) Huarng, J. C.; Min, K.; White, J. L. *Polym. Eng. Sci.* **1988**, *28*, 1590–1599.
(59) Nishio, Y.; Manley, R. J. *Polym. Eng. Sci.* **1990**, *30*, 71–82.
(60) Nojima, S.; Hashizume, K.; Rohadi, A.; Sasaki, S. *Polymer* **1997**, *38*, 2711–2718.
(61) Chatani, Y.; Okita, Y.; Tadokoro, H.; Yamashita, Y. *Polym. J.* **1970**, *1*, 555–562.
(62) Bittinger, H.; Marchesault, H. *Acta Crystallogr.* **1970**, *B26*, 1923–1927.
(63) Hu, H.; Dorset, D. L. *Macromolecules* **1990**, *23*, 4604–4607.
(64) Kasai, N.; Kakudo, M. In *X-ray diffraction by Macromolecules*; Springer: Heidelberg, 2005; Vol. 80, p 504.
(65) Chu, B.; Hsiao, B. *Chem. Rev.* **2001**, *101*, 1727–1761.
(66) Putnam, C. D.; Hammel, M.; Hura, G. L.; Tainer, J. A. *Q. Rev. Biophys.* **2007**, *40*, 191–285.
(67) Le Fevere de Ten Hove, C.; Penelle, J.; Ivanov, D. A.; Jonas, A. M. *Nature Mater.* **2004**, *3*, 33–37.
(68) Xiong-Feng, T.; Xiao-Jin, W.; Xue-Mei, Z.; Nan, X.; Wei, W.; Gerhard, W.; Zhong-Hua, W. *Macromolecules* **2007**, *40*, 4386–4388.
(69) Jun-Ting, X.; Yu-Jin, Z.; Zhi-Qiang, F. *J. Appl. Crystallogr.* **2004**, *37*, 295–299.
(70) Glatter, O. *J. Appl. Crystallogr.* **1980**, *13*, 577–584.
(71) Jeong, J.-C.; Lee, J.; Cho, K. *J. Controlled Release* **2003**, *92*, 249–258.
(72) He, C.; Sun, J.; Ma, J.; Chen, X.; Jing, X. *Biomacromolecules* **2006**, *7*, 3482–3489.
(73) Hura, G. L.; Menon, A. L.; Hammel, M.; Rambo, R. P.; Poole, F. L., II; Tsutakawa, S. E.; Jenney, F. E., Jr.; Classen, S.; Frankel, K. A.; Hopkins, R. C.; Yang, S-j.; Scott, J. W.; Dillard, B. D.; Adams, M. W. W.; Tainer, J. A. *Nature Methods* **2009**, *6*, 606–612.
(74) Lord, T. D.; Hobbs, J. K.; Terry, A. E.; Kvick, Å.; Hanna, S. *Macromolecules* **2010**, *43*, 3365–3375.
(75) Glatter, O. *J. Appl. Crystallogr.* **1977**, *10*, 415–421.
(76) Berrill, S. A.; Heatley, F.; Collett, J. H.; Attwood, D.; Booth, C.; Fairclough, J. P. A.; Ryan, A. J.; Viras, K.; Dutton, A. J.; Blundell, R. S. *J. Mater. Chem.* **1999**, *9*, 1059–1063.
(77) Mykhaylik, O. O.; Ryan, A. J.; Tzokova, N.; Williams, N. *J. Appl. Crystallogr.* **2007**, *40*, 506–511.
(78) Socrates, G. In *Infrared Characteristic Group Frequencies: Tables and Charts*; John Wiley and Sons: New York, 2004; p 366.
(79) Cramer, N. B.; Bowman, C. N. *J. Polym. Sci., Part A: Polym. Chem.* **2001**, *39*, 3311–3319.
(80) Stubenrauch, K.; Fritz-Popovski, G.; Ingolić, E.; Grogger, W.; Glatter, O.; Stelzer, F.; Trimmel, G. *Macromolecules* **2007**, *40*, 4592–4600.

NOTE ADDED AFTER ASAP PUBLICATION

This article posted ASAP on June 16, 2011. Figure 1 has been revised. The correct version posted on June 21, 2011.